On the dynamics through a conical intersection

Basile F. E. Curchod[†] and Federica Agostini[*,‡]

[†]*Centre for Computational Chemistry, School of Chemistry, University of Bristol, Bristol BS8 1TS, UK*

[‡]*Laboratoire de Chimie Physique, UMR 8000 CNRS/University Paris-Sud, University Paris-Saclay, 91405 Orsay, France*

E-mail: federica.agostini@u-psud.fr

Abstract

Conical intersections represent critical topological features of potential energy surfaces and open ultrafast nonradiative deactivation channels for photoexcited molecules. In the following, we investigate how this funneling picture is transposed in the eyes of the exact factorization formalism for a two-dimensional model system. The exact factorization of the total molecular wavefunction leads to the fundamental concept of time-dependent potential energy surface and time-dependent vector potential, whose behavior during a dynamics through a conical intersection has up to now remained unexplored. Despite the fact that these quantities might be viewed as time-dependent generalizations of the adiabatic potential energy surfaces and the nonadiabatic coupling vectors – characteristic quantities appearing in the Born-Oppenheimer framework – we observe that they do not exhibit particular topological features in the region of conical intersection, but still reflect the complex dynamics of the nuclear wavepacket.

Graphical TOC Entry

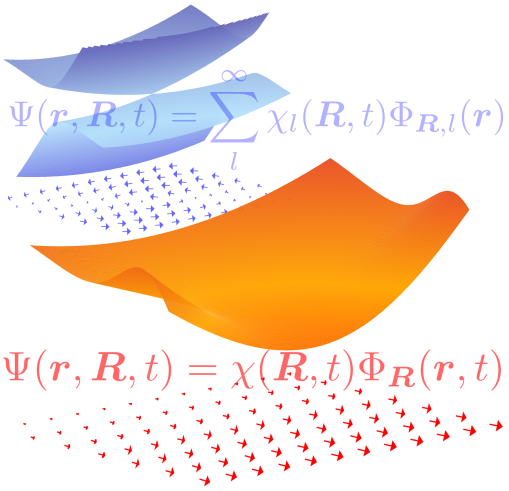

Keywords

Conical intersection, Nonadiabatic dynamics, Exact factorization

Light absorption in molecular systems triggers a highly nonequilibrium dynamics, most of the time combined with the appearance of nonadiabatic effects attesting from the breakdown of the Born-Oppenheimer (BO) approximation. Dynamics through so-called "conical intersections" perfectly exemplify the strong interplay between electronic and nuclear motion in excited-state dynamics.[1,2] Conical intersections (CIs) are related to regions of molecular configuration space for which two (or more) electronic states become degenerate. Only a set of two nuclear coordinates can linearly lift this degeneracy, leading to the formation of a characteristic double-cone shape in the so-called branching space. Any other nuclear displacements in the intersection space (defined by the remaining $3N_n - 8$ coordinates, with N_n the number of nuclei) preserve degeneracy between electronic states. As such, CIs act as efficient funnels between electronic states, allowing a photoexcited molecule to relax between electronic states efficiently.[3–9]

While Teller predicted this feature of potential energy surfaces (PESs) in 1937[10] – only ten years after the seminal article of Born and Oppenheimer[11] – the relevance of CIs in photochemical processes was only notified decades after,[12,13] further supported by extensive theoretical analysis.[1,2,14–27] The picture of CIs in molecular systems is, however, a result of the so-called electronic "adiabatic representation" – in which electronic wavefunctions are represented by eigensolutions of the electronic (time-independent) Schrödinger equation. The characteristic conical shape of potential energy surfaces indeed disappears in a diabatic representation of the electronic state, in which the nuclear kinetic energy operator becomes diagonal. Hence, the funnel picture of CIs is rooted in a particular representation of the electronic wavefunctions.

More critical is the question of the *dynamics* of a nuclear wavepacket through a CI. The present Letter focuses on this particular topic, analyzed in the perspective of the exact factorization (EF).[28,29] Previous work[30] on a related topic, but from a time-independent viewpoint, has shown how typical features connected to CIs between adiabatic PESs and/or to molecular geometric phases disappear in the EF, and how such features re-emerge only in

the "BO limit",[31] or infinite-mass limit[30] (except if one chooses current-carrying eigenstates in systems with degeneracies[32]). Here, the dynamical perspective – that has so far remained unexplored – will be investigated by reporting the key differences between the EF formalism and the adiabatic representation.

In the EF, the solution of the time-dependent Schrödinger equation $\hat{H}(\boldsymbol{r},\boldsymbol{R})\Psi(\boldsymbol{r},\boldsymbol{R},t) = i\hbar\partial_t\Psi(\boldsymbol{r},\boldsymbol{R},t)$, i.e., the molecular wavefunction, is written as a single product $\Psi(\boldsymbol{r},\boldsymbol{R},t) = \chi(\boldsymbol{R},t)\Phi_{\boldsymbol{R}}(\boldsymbol{r},t)$ of a nuclear wavefunction and an electronic factor, with parametric dependence on the nuclear configuration. The whole set of electronic and nuclear coordinates is indicated as $\boldsymbol{r},\boldsymbol{R}$, respectively, and the molecular Hamiltonian $\hat{H}(\boldsymbol{r},\boldsymbol{R}) = \hat{T}_n(\boldsymbol{R}) + \hat{H}_{BO}(\boldsymbol{r},\boldsymbol{R})$ comprises the nuclear kinetic energy, $\hat{T}_n(\boldsymbol{R})$, and the electronic BO Hamiltonian, $\hat{H}_{BO}(\boldsymbol{r},\boldsymbol{R})$, containing the electronic kinetic energy and all the interactions. The partial normalization condition on the electronic wavefunction, $\int d\boldsymbol{r}|\Phi_{\boldsymbol{R}}(\boldsymbol{r},t)|^2 = 1$, $\forall\boldsymbol{R},t$, guarantees the uniqueness of the factored form of $\Psi(\boldsymbol{r},\boldsymbol{R},t)$ up to within a $(\boldsymbol{R},t)$-dependent phase transformation, and that $|\chi(\boldsymbol{R},t)|^2$ yields the exact nuclear many-body density. In addition, $\chi(\boldsymbol{R},t)$ yields as well the exact nuclear many-body current density. As a result of the EF, the time-dependent Schrödinger equation is decomposed as coupled evolution equations for the two components of the molecular wavefunction, namely

$$\left(\hat{H}_{BO}(\boldsymbol{r},\boldsymbol{R}) + \hat{U}_{en}^{coup}[\Phi_{\boldsymbol{R}},\chi] - \epsilon(\boldsymbol{R},t)\right)\Phi_{\boldsymbol{R}}(\boldsymbol{r},t) = i\hbar\partial_t\Phi_{\boldsymbol{R}}(\boldsymbol{r},t) \tag{1}$$

$$\left(\sum_{\nu=1}^{N_n}\frac{\left[-i\hbar\nabla_\nu + \boldsymbol{A}_\nu(\boldsymbol{R},t)\right]^2}{2M_\nu} + \epsilon(\boldsymbol{R},t)\right)\chi(\boldsymbol{R},t) = i\hbar\partial_t\chi(\boldsymbol{R},t)\,. \tag{2}$$

The nuclear equation is a standard time-dependent Schrödinger equation, with time-dependent vector $\boldsymbol{A}_\nu(\boldsymbol{R},t)$ and scalar $\epsilon(\boldsymbol{R},t)$ potentials accounting for the (nonadiabatic) effect of the electrons. More details on $\boldsymbol{A}_\nu(\boldsymbol{R},t)$ and $\epsilon(\boldsymbol{R},t)$ will be given below, being the central quantities of interest for our analysis of dynamics through CIs. The electronic equation describes how the electronic wavefunction follows nuclear evolution, containing the full dynamical coupling to the nuclear degrees of freedom, encoded in the operator $\hat{U}_{en}^{coup}[\Phi_{\boldsymbol{R}},\chi]$ (for further

information on this operator, the interested reader is referred to Refs.[28,29,33,34]).

The EF, both in its static[30,32,35–50] and dynamical formulations,[28,29,33,51–62] has been employed for a large variety of purposes, from the rationalization of electron-nuclear correlation[31,36,44,50,63] to the interpretation of nonadiabatic processes in molecular systems,[33,55,59,61,64] mainly via the analysis of the vector and scalar potentials of the theory. The common aim of those analysis has been, and still is, to explore new avenues for the development of algorithms for excited-state dynamics. In this Letter we proceed along similar lines and focus on the dynamics through a CI, which offers the opportunity to deploy for the first time the EF formalism to nonadiabatic processes in more than one dimension.

In the time-independent case, it has been shown[30] that when two adiabatic PESs present a CI the scalar potential from the EF does not manifest any singular behavior, rather it acquires a diabatic-like character that completely overlooks the presence of the CI. Does this feature persist during the dynamics? What happens far away from the CI, where dynamics is supposed to happen "adiabatically"? These questions will be addressed below. Furthermore, previous analysis have focused either on one-dimensional problems[28,29,33,51,52,56,57,61] or on static situations[30] where the electronic factor in the EF is real. Both cases yield a trivial vector potential. In a general situation, however, the effect of the vector potential shall be accounted for, especially in a dynamical situation. Then, how does the vector potential look like? Does it manifest any common feature with its "adiabatic counterpart", i.e., the nonadiabatic coupling vectors, which are singular at the CI? In the following, the vector potential will be also discussed.

To address these different questions, we performed numerically exact quantum dynamics simulations for a two-state two-dimensional system, constructed from a model of the isomerization of retinal in rhodopsin[65,66] (see Computational Details for more information). We stress here that we adopted this model with the only intention of studying a dynamics through CIs. Therefore, we are not going to comment on the implications of our findings for the chemical system this model depicts. The relevant portion of the model adiabatic PESs is

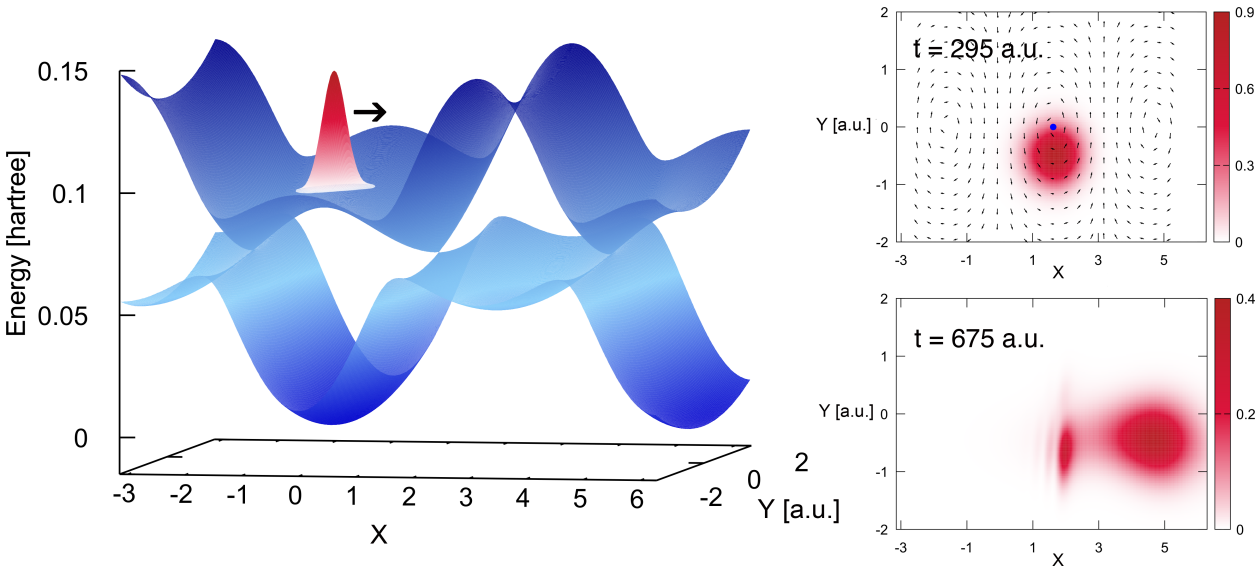

Figure 1: Left: Schematic representation of the interesting portion of the model adiabatic potential energy surfaces used in this work. Right: Total nuclear density $|\chi(\boldsymbol{R},t)|^2$ around the CI (t = 295 a.u., upper panel), and after bifurcation (t = 675 a.u., lower panel). The direction of the nonadiabatic coupling vectors $\boldsymbol{d}_{12}(\boldsymbol{R})$ are represented as a vector field in the right upper panel, and a blue dot highlights the location of the CI of interest.

depicted in Fig. 1 (left) and characterized by two effective coordinates, $\boldsymbol{R} = (X, Y)$, X being the reactive coordinate towards the CI. The initial Gaussian wavepacket is initialized in the excited state and sent towards a CI located at $\boldsymbol{R}_{CI} = (1.63, 0.0)$ with an initial momentum $\boldsymbol{P}_{ini} = (10.0, 0.0)$. We chose this set of initial conditions for two reasons: (i) the initial nuclear wavepacket will rapidly enter the CI region, leading to an almost complete population transfer to the ground state (state 1), and (ii) a small portion of the wavepacket remains in state 2 after the CI, leading eventually to a wavepacket bifurcation. Hence, we will focus in the following on two particular snapshots during the simulated quantum dynamics. At t = 295 a.u. (Fig. 1, upper right panel), the nuclear wavepacket evolves on the BO PES 2 in the neighborhood of the CI and starts to transfer population onto the BO PES 1. At t = 675 a.u. (Fig. 1, lower right panel), the nuclear wavepacket has left the first CI region and is entering a second coupling region. However, the nuclear wavepacket components in state 2 and 1 also start to spatially separate due to the differences in the PESs topology – a bifurcation takes place.

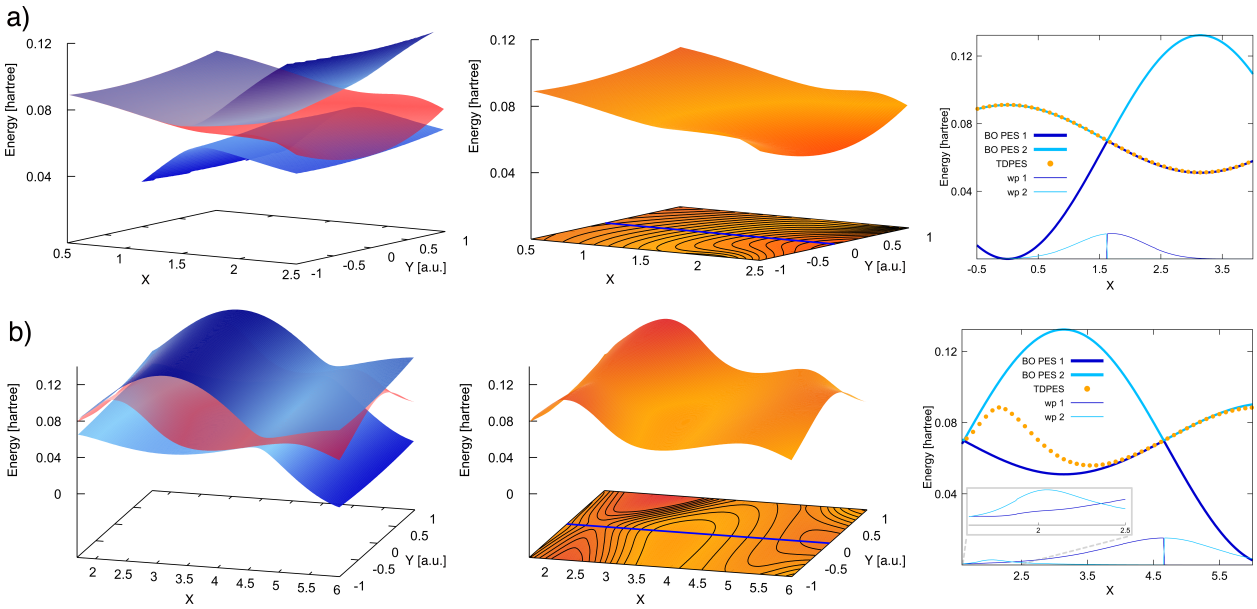

Figure 2: Gauge-invariant part of the TDPES at two different times of the simulation. a) At $t = 295$ a.u.: the total nuclear wavefunction is in the neighborhood of the CI. b) At $t = 675$ a.u.: a bifurcation of the total nuclear wavefunction is taking place. Left panel: comparison of the Born-Oppenheimer (adiabatic) PESs (in blue) with the TDPES (in red). Middle panel: TDPES, with the corresponding contour map. Right panel: TDPES, BO PESs, and nuclear densities in state 1 and 2 – $|\chi_1(\boldsymbol{R},t)|^2$ and $|\chi_2(\boldsymbol{R},t)|^2$ – along a cut in the X direction (indicated by a blue line in the middle panel). The inset in the lower right panel represents a zoom on the nuclear densities in the region of bifurcation.

Let us now turn to the EF representation of this dynamics through a CI. The time-dependent scalar potential, or time-dependent PES (TDPES), is defined as

$$\epsilon(\boldsymbol{R},t) = \langle \Phi_{\boldsymbol{R}}(t)|\hat{H}_{BO} + \hat{U}_{en}^{coup} - i\hbar\partial_t|\Phi_{\boldsymbol{R}}(t)\rangle_{\boldsymbol{r}}\,, \tag{3}$$

with $\langle \ldots \rangle_{\boldsymbol{r}}$ indicating an integration over electronic coordinates.[1] The first two terms do not depend on the choice of the $(\boldsymbol{R},t)$-dependent gauge, i.e., they are gauge invariant, while the last term depends on the choice of gauge. In this Letter, only the first gauge-invariant term of the TDPES will be analyzed. In fact, the remaining terms do not develop any peculiar feature in the chosen gauge (introduced below), as they (i) cancel each other when the nuclear wavepacket passes through the conical intersection, and (ii) produce a small "bump" when

[1] In this particular case, it is a sum over the discrete set of electronic states.

the nuclear wavepacket splits. An analytical justification of this observation is currently under investigation. It follows that only the term $\langle\Phi_{\boldsymbol{R}}(t)|\hat{H}_{BO}|\Phi_{\boldsymbol{R}}(t)\rangle_{\boldsymbol{r}}$ exhaustively reflects in the TDPES the behavior of the nuclear density in the dynamics presented here.[51,52] The first panel of Fig. 2a compares the adiabatic BO PESs (blue) to the TDPES (red) when the nuclear wavepacket is passing through the CI ($t = 295$ a.u.). The conical shape formed by the adiabatic PESs is clearly absent from the TDPES, which shows a smooth character, bridging the two adiabatic surfaces diabatically (Fig. 2a, middle panel). A cut along the X coordinate, depicted by a blue line in the middle panel of Fig. 2a, facilitates the comparison between the adiabatic PESs and the TDPES. In this one-dimensional representation (Fig. 2a, right panel), it becomes evident that the TDPES perfectly follows a diabatic character, merging in the region of the CI the topology of the adiabatic BO PESs 2 and 1. This smooth and structureless picture of the TDPES is, however, altered at $t = 675$ a.u., after the crossing through the CI (Fig. 2b). At this particular time, the TDPES follows the adiabatic surfaces in some region of the configuration space, but also exhibits additional features directly related to the underlying nuclear wavepacket dynamics. As observed in the one-dimensional cut (Fig. 2b, right panel), a component of the nuclear wavefunction on the BO PES 2 has indeed been reflected in the region $X < 3.0$ (see inset in the right panel of Fig. 2b). This reflection leads to a splitting of the total nuclear wavefunction (Fig. 1, lower right panel) that the TDPES enforces by slowly developing a step, which will eventually bridge the BO PES 2 with the BO PES 1. This step is clearly apparent in a one-dimensional cut along the X coordinate (Fig. 2b, right panel, in the region $2.2 < X < 3.5$). We note that the overlap between the TDPES and the BO PES 2 in the $X < 3.0$ region is not total as the nuclear wavefunction component in state 1 is non-zero in this region. To summarize, the dynamics of a nuclear wavepacket through a CI is characterized in the EF by a smooth gauge-independent TDPES exhibiting a diabatic character; the TDPES will, however, develop peculiar structures if a wavepacket bifurcation occurs after the CI.

The behavior of the TDPES presented above extends the observations performed on one-

dimensional systems to a more general case involving dynamics through CIs. However, the EF formalism is not only concerned with the TDPES, but also introduces a time-dependent vector potential

$$\boldsymbol{A}_\nu(\boldsymbol{R},t) = \langle\Phi_{\boldsymbol{R}}(t)| - i\hbar\nabla_\nu|\Phi_{\boldsymbol{R}}(t)\rangle_{\boldsymbol{r}} \tag{4}$$

(we have $\boldsymbol{A}(\boldsymbol{R},t) = \boldsymbol{A}(X,Y,t)$ in the present case[2] with $\nu = 1$). In a one-dimensional case, this vector potential could easily be gauged away – a strategy followed in most previous works on the EF. However, such a choice of gauge is not general enough to be applied on systems in higher dimensions. In the following, we fix the gauge by imposing that the phase of the nuclear wavefunction $S(\boldsymbol{R},t) = 0$, i.e., the nuclear wavefunction given by $\chi(\boldsymbol{R},t) = |\chi(\boldsymbol{R},t)|e^{iS(\boldsymbol{R},t)/\hbar}$ is real and non-negative in this gauge. As a direct consequence of this choice of gauge, all the complex contributions to the total molecular wavefunction are transferred to the electronic wavefunction, and the time-dependent vector potential corresponds to $\boldsymbol{A}(\boldsymbol{R},t) = \langle\Phi_{\boldsymbol{R}}(t)| - i\hbar\nabla|\Phi_{\boldsymbol{R}}(t)\rangle_{\boldsymbol{r}} = \frac{\Im\langle\Psi(\boldsymbol{R},t)|\nabla|\Psi(\boldsymbol{R},t)\rangle_{\boldsymbol{r}}}{|\chi(\boldsymbol{R},t)|^2}$, where $\Im\langle\Psi(\boldsymbol{R},t)|\nabla|\Psi(\boldsymbol{R},t)\rangle_{\boldsymbol{r}}$ (divided by the nuclear mass) is the true nuclear many-body current density. It is worth stressing here that, despite $\boldsymbol{A}(\boldsymbol{R},t)$ being a gauge-dependent quantity, it acquires in the chosen gauge a special meaning, as it is the (observable) nuclear current density. Furthermore, as it follows from its definition, the vector potential might be viewed as a generalization of the concept of nonadiabatic couplings in the EF formalism. As a result of the previous considerations, the behavior of $\boldsymbol{A}(\boldsymbol{R},t)$ during a funneling through a CI deserves a thorough analysis.

The vector potential $\boldsymbol{A}(\boldsymbol{R},t)$ does not show any singularity when the nuclear wavepacket reaches the CI (Fig. 3), mostly pointing towards positive X values. Bearing in mind its relationship with the true nuclear current density, the overall behavior of the vector potential reflects that the nuclear wavefunction is mostly travelling towards positive X values, with

[2]The vector potential has the dimensionality of the nuclear configuration space, i.e., it is a $3N_n$-dimensional vector. For the model system presented here, we expect the vector potential to be a 2-component vector. Therefore, we can either set $\nu = 1$ and associate two Cartesian components, x and y, to the "nucleus" ν, as done here, or set $\nu = 2$ and associate one Cartesian component to each value of ν.

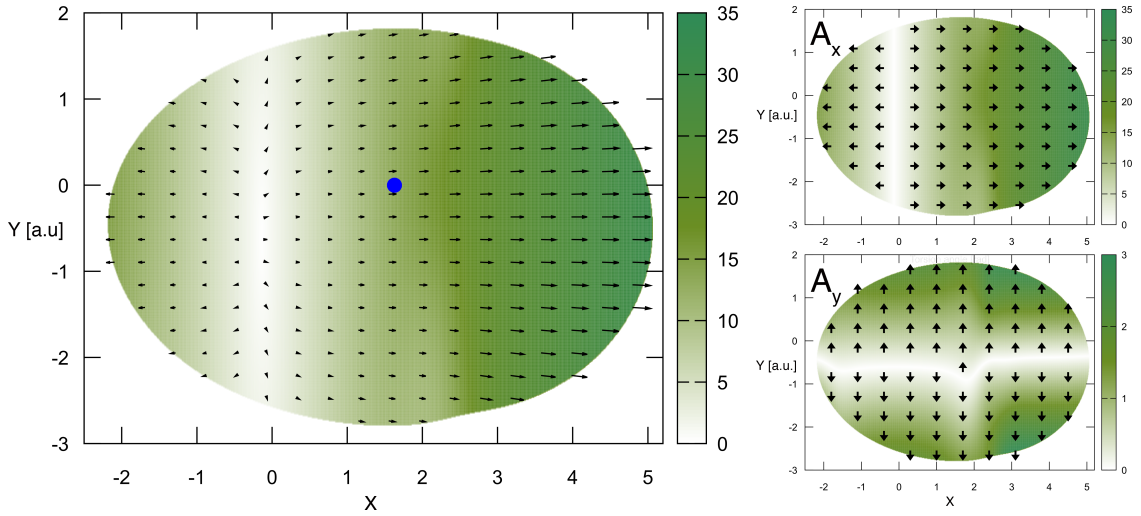

Figure 3: Left: representation of the time-dependent vector potential $\boldsymbol{A}(\boldsymbol{R},t)$ at $t = 295$ a.u., in the region where $|\chi(\boldsymbol{R},t)|^2 > 10^{-10}$. The colormap indicates the magnitude of the vector field, and a blue dot highlights the location of the CI of interest. Right: $A_x(\boldsymbol{R},t)$ (top) and $A_y(\boldsymbol{R},t)$ (bottom) components of the time-dependent vector potential. Arrows have a fixed length and indicate the direction of the field component.

a slight expansion in the Y coordinate. Breaking $\boldsymbol{A}(\boldsymbol{R},t)$ into its $A_x(\boldsymbol{R},t)$ and $A_y(\boldsymbol{R},t)$ components (Fig. 3, right panels) confirms this overall trend in the vector field.

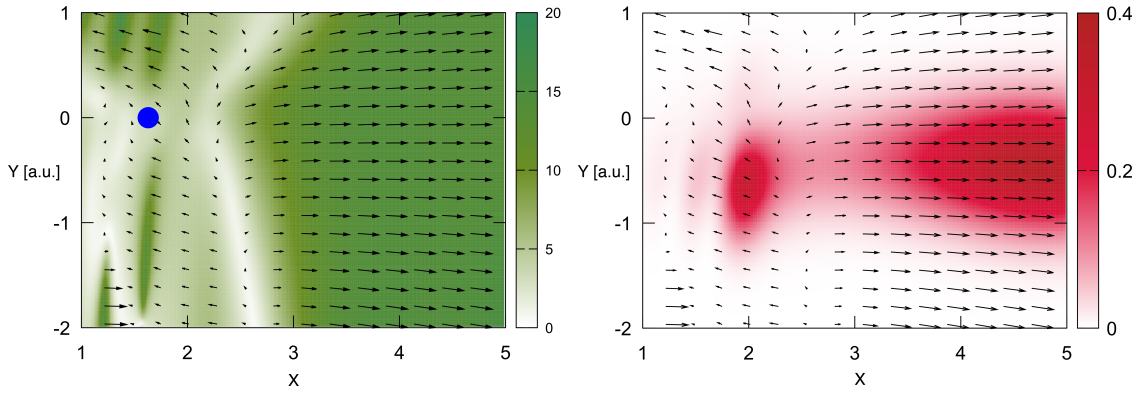

Figure 4: Left: representation of the time-dependent vector potential $\boldsymbol{A}(\boldsymbol{R},t)$ at $t = 675$ a.u., in the region where $|\chi(\boldsymbol{R},t)|^2 > 10^{-10}$. The colormap indicates the magnitude of the vector field, and a blue dot highlights the location of the CI of interest. Right: time-dependent vector potential superimposed on the total nuclear density $|\chi(\boldsymbol{R},t)|^2$.

The behavior of the vector potential, and its relation to the nuclear wavepacket dynamics, becomes even clearer at the time of bifurcation (Fig. 4). The direction of $\boldsymbol{A}(\boldsymbol{R},t)$ indeed reflects the complex dynamics where the main component of the nuclear wavepacket ($3 <$

$X < 5$) evolves towards positive X in state 1, while a smaller wavepacket in state 2 (centered at $X = 2$) is bouncing back towards the CI. As $\boldsymbol{A}(\boldsymbol{R}, t)$ is the nuclear current density, the vector field clearly exhibits changes of direction as a result of this bifurcation. In addition, $\boldsymbol{A}(\boldsymbol{R}, t)$ appears to have a non-vanishing curl during the dynamics,[3] a property that does not depend on a particular choice of gauge, as $\nabla \times \tilde{\boldsymbol{A}}(\boldsymbol{R}, t) = \nabla \times (\boldsymbol{A}(\boldsymbol{R}, t) + \nabla\theta(\boldsymbol{R}, t)) = \nabla \times \boldsymbol{A}(\boldsymbol{R}, t)$ (with $\theta(\boldsymbol{R}, t)$ the gauge phase and $\tilde{\boldsymbol{A}}$ is the gauge-transformed vector potential[33]). This result shall be considered of general validity, as only in a highly symmetric situation one might expect to obtain a nuclear current density, i.e., a vector potential, with vanishing curl. Therefore, the time-dependent vector potential of the EF cannot be in general gauged away. We finally note that the curl of the vector potential does not appear to present any peculiar feature related to the CI.

Overall, both the time-dependent potential energy surface and the time-dependent vector potential do not present any peculiar feature connected to conical intersections. From a practical point of view, this result is extremely encouraging, as it proves that working in the exact factorization framework greatly simplifies the description of nonadiabatic processes, even in the presence of CIs that lead in the adiabatic representation to singular nonadiabatic coupling vectors and – as recently noted – even more problematic singular diagonal second-order couplings.[64,67] The reported analysis confirms that the development of (quantum-classical trajectory-based) algorithms[68–73] to simulate excited-state dynamics can easily proceed in such a representation-free framework. The gauge introduced in this work has also its advantage from a quantum-classical perspective: the nuclear wavefunction contains information *only* about the nuclear density, whose evolution can be easily mimicked by classical trajectories (or frozen/thawed Gaussians). Phase information, and consequently information about the nuclear velocity field, is totally encoded in the electronic wavefunction, i.e., in the time-dependent vector potential, as shown in this work. Purely classical trajectories can be employed to follow the evolution of the nuclear wavefunction in the present gauge, without

[3]If the flux of the curl of the vector potential is computed on a surface whose boundary encircles the position of the CI, one obtains a value that is not "quantized" and will depend on the choice of the surface.

the need of refining the dynamics with semiclassical-like phase corrections. This simplified nuclear dynamics comes at the cost of introducing a vector potential contribution to the nuclear Hamiltonian. The vector potential is, however, a well-behaving function, that introduces no numerical complications. It is worth noting that all quantities are smooth functions of nuclear coordinates if the nuclear wavefunction does not present nodes, for example resulting from strong interference effects as recently described for nonadiabatic processes.[61] From a quantum-mechanical point of view this might seem a severe restriction, but it is indeed important to keep in mind that the probability of finding classical trajectories in a region of zero probability is very small.

In summary, the time-dependent potential energy surface shown in the Letter dynamically switches from a diabatic shape to a series of steps that either connect or are "enclosed" by the adiabatic surfaces. Transitions between diabatic and adiabatic character are not imposed, but they are features arising directly from the dynamics. Furthermore, the time-dependent potential energy surface remains at all times a smooth function of nuclear coordinates. We also introduced for the first time a gauge where the time-dependent vector potential is non-zero. Such vector potential is as well a smooth function of nuclear coordinates. Being related to the nuclear velocity field, the dynamics naturally leads to a situation where the vector potential develops a non-zero curl – a gauge-independent quantity. Therefore, the vector potential provides information on the nuclear current that cannot be accounted for by any choice of the nuclear phase.

Computational details

The initial nuclear wavepacket is taken as Gaussian, with widths $\sigma_X = 0.05$ and $\sigma_Y = 0.2$, and is centered at $\boldsymbol{R}_{ini} = (0.0, -0.5)$. We first solve the full time-dependent Schrödinger equation numerically using a split-operator formalism[74] in a diabatic basis. The 2-by-2 Hamiltonian is given by

$$\hat{\boldsymbol{H}}(X,Y) = -\frac{1}{2m}(\partial_X^2+\partial_Y^2)\mathbf{1}_2+\begin{pmatrix} \frac{1}{2}W_1\left(1-cos(X)\right)+\frac{\omega}{2}Y^2 & \lambda Y \\ \lambda Y & E_1-\frac{1}{2}W_2\left(1-cos(X)\right)+\frac{\omega}{2}Y^2+\kappa Y \end{pmatrix} \tag{5}$$

with $W_1 = 0.1323$, $\omega = 0.007$, $m = 2000.0$, $E1 = 0.091$, $W_2 = 0.040$, $\lambda = 0.007$, and $\kappa = 0.0037$. All quantities (parameters and coordinates) are given in atomic units, and the coordinate X is dimensionless. This model is adapted from the one presented in Refs.[65,66]

We then reconstructed the TDPES and the time-dependent vector potential from the time-dependent nuclear wavefunctions $\chi_l(\boldsymbol{R},t)$, with $l = 1, 2$, using the relation $\chi(\boldsymbol{R},t) = \sqrt{|\chi_1(\boldsymbol{R},t)|^2+|\chi_2(\boldsymbol{R},t)|^2}$. The coefficients of the electronic wavefunction in the diabatic basis are then given as $\chi_l(\boldsymbol{R},t)/\chi(\boldsymbol{R},t)$. Using the fact that nonadiabatic coupling vectors are identically zero in the diabatic basis, we provide the general expressions of the gauge-invariant, ϵ_{GI}, and gauge-dependent, ϵ_{GD}, parts of the TDPES and of the vector potential in this basis, namely $\epsilon_{GI} = \sum_{l,k}(\chi_k^*\chi_l/|\chi|^2)V_{kl} + \sum_\nu(\hbar^2/2M_\nu)\sum_l|\nabla_\nu(\chi_l/\chi)|^2 - \sum_\nu(\mathbf{A}_\nu^2/2M_\nu)$, $\epsilon_{GD} = -i\hbar\sum_l(\chi_l/\chi)^*\partial_t(\chi_l/\chi)$ and $\mathbf{A}_\nu = -i\hbar\sum_l(\chi_l/\chi)^*\nabla_\nu(\chi_l/\chi)$, where the symbol V_{kl} indicates the elements of the electronic Hamiltonian in the diabatic basis and l, k label the states. It is worth pointing out that the two EF quantities of interest here do not depend on a particular choice of electronic representation.

Acknowledgement

We are grateful to David Lauvergnat for stimulating discussions, and we acknowledge the COST Action MP1306 "EUSpec" for the funding of a Short Term Scientific Mission that initiated this work.

References

(1) Yarkony, D. R. Diabolical conical intersections. *Rev. Mod. Phys.* **1996**, *68*, 985.

(2) Domcke, W., Yarkony, D., Köppel, H., Eds. *Conical Intersections: Electronic Structure, Dynamics & Spectroscopy*; World Scientific Pub Co Inc, 2004; Vol. 15.

(3) Ashfold, M. N.; Devine, A. L.; Dixon, R. N.; King, G. A.; Nix, M. G.; Oliver, T. A. Exploring nuclear motion through conical intersections in the UV photodissociation of phenols and thiophenol. *Proc. Natl. Acad. Sci. USA.* **2008**, *105*, 12701.

(4) Polli, D.; Altoè, P.; Weingart, O.; Spillane, K. M.; Manzoni, C.; Brida, D.; Tomasello, G.; Orlandi, G.; Kukura, P.; Mathies, R. A. et al. Conical intersection dynamics of the primary photoisomerization event in vision. *Nature* **2010**, *467*, 440.

(5) Wörner, H.; Bertrand, J.; Fabre, B.; Higuet, J.; Ruf, H.; Dubrouil, A.; Patchkovskii, S.; Spanner, M.; Mairesse, Y.; Blanchet, V. et al. Conical intersection dynamics in NO2 probed by homodyne high-harmonic spectroscopy. *Science* **2011**, *334*, 208.

(6) Duan, H.-G.; Thorwart, M. Quantum Mechanical Wave Packet Dynamics at a Conical Intersection with Strong Vibrational Dissipation. *J. Phys. Chem. Lett.* **2016**, *7*, 382.

(7) Ben-Nun, M.; Martínez, T. J. Photodynamics of ethylene: Ab initio studies of conical intersections. *Chem. Phys.* **2000**, *259*, 237–248.

(8) Spezia, R.; Burghardt, I.; Hynes, J. T. Conical intersections in solution: non-equilibrium versus equilibrium solvation. *Mol. Phys.* **2006**, *104*, 903–914.

(9) Burghardt, I.; Cederbaum, L. S.; Hynes, J. T. Environmental effects on a conical intersection: A model study. *Faraday Discuss.* **2004**, *127*, 395–411.

(10) Teller, E. The Crossing of Potential Surfaces. *J. Phys. Chem.* **1937**, *41*, 109–116.

(11) Born, M.; Oppenheimer, R. Zur Quantentheorie der Molekeln. *Annalen der Physik* **1927**, *389*, 457–484.

(12) Michl, J.; Bonačić-Koutecký, V. *Electronic Aspects of Organic Photochemistry*; John Wiley and Sons, New York, 1990.

(13) Michl, J. Photochemical reactions of large molecules. I. A simple physical model of photochemical reactivity. *Mol. Photochem.* **1972**, *4*, 243–257.

(14) Mead, C. A.; Truhlar, D. G. On the determination of Born–Oppenheimer nuclear motion wave functions including complications due to conical intersections and identical nuclei. *J. Chem. Phys.* **1979**, *70*, 2284–2296.

(15) Berry, M. V.; Wilkinson, M. Diabolical points in the spectra of triangles. Proc. Roy. Soc. London Ser. A. 1984; pp 15–43.

(16) Berry, M. V. Quantal phase factors accompanying adiabatic changes. Proc. Roy. Soc. London Ser. A. 1984; pp 45–57.

(17) Bernardi, F.; Olivucci, M.; Robb, M. A. Potential energy surface crossings in organic photochemistry. *Chem. Soc. Rev.* **1996**, *25*, 321–328.

(18) Yarkony, D. R. Conical Intersections: The New Conventional Wisdom. *J. Phys. Chem.* **2001**, *105*, 6277.

(19) Worth, G. A.; Cederbaum, L. S. Beyond Born-Oppenheimer: molecular dynamics through a conical intersection. *Annu. Rev. Phys. Chem.* **2004**, *55*, 127–158.

(20) Baer, M. *Beyond Born-Oppenheimer: Electronic Nonadiabatic Coupling Terms and Conical Intersections*; John Wiley & Sons, Inc., 2006.

(21) Levine, B. G.; Martínez, T. J. Isomerization through conical intersections. *Annu. Rev. Phys. Chem.* **2007**, *58*, 613–634.

(22) Martinez, T. J. Physical chemistry: Seaming is believing. *Nature* **2010**, *467*, 412–413.

(23) Matsika, S.; Krause, P. Nonadiabatic events and conical intersections. *Annu. Rev. Phys. Chem.* **2011**, *62*, 621.

(24) Domcke, W.; Yarkony, D. R. Role of conical intersections in molecular spectroscopy and photoinduced chemical dynamics. *Annu. Rev. Phys. Chem.* **2012**, *63*, 325–352.

(25) Domcke, W., Yarkony, D., Köppel, H., Eds. *Conical Intersections: Theory, Computation and Experiment*; World Scientific Pub Co Inc, 2012; Vol. 17.

(26) Malhado, J. P.; Bearpark, M. J.; Hynes, J. T. Non-adiabatic dynamics close to conical intersections and the surface hopping perspective. *Frontiers in chemistry* **2014**, *2*, 97.

(27) Zhu, X.; Yarkony, D. R. Non-adiabaticity: the importance of conical intersections. *Mol. Phys.* **2016**, *114*, 1983.

(28) Abedi, A.; Maitra, N. T.; Gross, E. K. U. Exact factorization of the time-dependent electron-nuclear wave function. *Phys. Rev. Lett.* **2010**, *105*, 123002.

(29) Abedi, A.; Maitra, N. T.; Gross, E. K. U. Correlated electron-nuclear dynamics: Exact factorization of the molecular wave-function. *J. Chem. Phys.* **2012**, *137*, 22A530.

(30) Min, S. K.; Abedi, A.; Kim, K. S.; Gross, E. K. U. Is the molecular Berry phase an artifact of the Born-Oppenheimer approximation? *Phys. Rev. Lett.* **2014**, *113*, 263004.

(31) Eich, F. G.; Agostini, F. The adiabatic limit of the exact factorization of the electron-nuclear wave function. *J. Chem. Phys.* **2016**, *145*, 054110.

(32) Requist, R.; Tandetzky, F.; Gross, E. K. U. Molecular geometric phase from the exact electron-nuclear factorization. *Phys. Rev. A* **2016**, *93*, 042108.

(33) Agostini, F.; Abedi, A.; Suzuki, Y.; Min, S. K.; Maitra, N. T.; Gross, E. K. U. The exact forces on classical nuclei in non-adiabatic charge transfer. *J. Chem. Phys.* **2015**, *142*, 084303.

(34) de Carvalho, F. F.; Bouduban, M. E. F.; Curchod, B. F. E.; Tavernelli, I. Nonadiabatic Molecular Dynamics Based on Trajectories. *Entropy* **2014**, *16*, 62.

(35) Hunter, G. Conditional probability amplitude analysis of coupled harmonic oscillators. *Int. J. Quantum Chem.* **1974**, *8*, 413.

(36) Hunter, G. Conditional probability amplitudes in wave mechanics. *Int. J. Quantum Chem.* **1975**, *9*, 237.

(37) Hunter, G. Ionization potentials and conditional amplitudes. *Int. J. Quantum Chem.* **1975**, *9*, 311.

(38) Bishop, D. M.; Hunter, G. Non-adiabatic potentials for H2+. *Mol. Phys.* **1975**, *30*, 1433.

(39) Bishop, D. M.; Cheung, L. M. Conditional probability amplitudes and the variational principle. *Chem. Phys. Lett.* **1977**, *50*, 172.

(40) Hunter, G. Nodeless wave function quantum theory. *Int. J. Quantum Chem.* **1980**, *9*, 133.

(41) Hunter, G. Nodeless wave functions and spiky potentials. *Int. J. Quantum Chem.* **1981**, *19*, 755.

(42) Hunter, G.; Tai, C. C. Variational marginal amplitudes. *Int. J. Quantum Chem.* **1982**, *21*, 1041.

(43) Hunter, G. The exact one-electron model of molecular structure. *Int. J. Quantum Chem.* **1986**, *29*, 197.

(44) Cederbaum, L. S. The exact molecular wavefunction as a product of an electronic and a nuclear wavefunction. *J. Chem. Phys.* **2013**, *138*, 224110.

(45) Gidopoulos, N. I.; Gross, E. K. U. Electronic non-adiabatic states: towards a density functional theory beyond the Born-Oppenheimer approximation. *Phil. Trans. R. Soc. A* **2014**, *372*, 20130059.

(46) Chiang, Y.-C.; Klaiman, S.; Otto, F.; Cederbaum, L. S. The exact wavefunction factorization of a vibronic coupling system. *J. Chem. Phys.* **2014**, *140*, 054104.

(47) Cederbaum, L. S. The exact wavefunction of interacting N degrees of freedom as a product of N single-degree-of-freedom wavefunctions. *Chem. Phys.* **2015**, *457*, 129.

(48) Lefebvre, R. Perturbations in vibrational diatomic spectra: Factorization of the molecular wave function. *J. Chem. Phys.* **2015**, *142*, 074106.

(49) Lefebvre, R. Factorized molecular wave functions: Analysis of the nuclear factor. *J. Chem. Phys.* **2015**, *142*, 214105.

(50) Requist, R.; Gross, E. K. U. Exact Factorization-Based Density Functional Theory of Electrons and Nuclei. *Phys. Rev. Lett.* **2016**, *117*, 193001.

(51) Abedi, A.; Agostini, F.; Suzuki, Y.; Gross, E. K. U. Dynamical steps that bridge piecewise adiabatic shapes in the exact time-dependent potential energy surface. *Phys. Rev. Lett* **2013**, *110*, 263001.

(52) Agostini, F.; Abedi, A.; Suzuki, Y.; Gross, E. K. U. Mixed quantum-classical dynamics on the exact time-dependent potential energy surfaces: A novel perspective on non-adiabatic processes. *Mol. Phys.* **2013**, *111*, 3625.

(53) Abedi, A.; Agostini, F.; Gross, E. K. U. Mixed quantum-classical dynamics from the exact decomposition of electron-nuclear motion. *Europhys. Lett.* **2014**, *106*, 33001.

(54) Agostini, F.; Abedi, A.; Gross, E. K. U. Classical nuclear motion coupled to electronic non-adiabatic transitions. *J. Chem. Phys.* **2014**, *141*, 214101.

(55) Suzuki, Y.; Abedi, A.; Maitra, N. T.; Yamashita, K.; Gross, E. K. U. Electronic Schrödinger equation with nonclassical nuclei. *Phys. Rev. A* **2014**, *89*, 040501(R).

(56) Agostini, F.; Min, S. K.; Gross, E. K. U. Semiclassical analysis of the electron-nuclear coupling in electronic non-adiabatic processes. *Ann. Phys.* **2015**, *527*, 546–555.

(57) Suzuki, Y.; Abedi, A.; Maitra, N. T.; Gross, E. K. U. Laser-induced electron localization in H_2^+: Mixed quantum-classical dynamics based on the exact time-dependent potential energy surface. *Phys. Chem. Chem. Phys.* **2015**, *17*, 29271–29280.

(58) Min, S. K.; Agostini, F.; Gross, E. K. U. Coupled-trajectory quantum-classical approach to electronic decoherence in nonadiabatic processes. *Phys. Rev. Lett.* **2015**, *115*, 073001.

(59) Khosravi, E.; Abedi, A.; Maitra, N. T. Exact Potential Driving the Electron Dynamics in Enhanced Ionization of H_2^+. *Phys. Rev. Lett.* **2015**, *115*, 263002.

(60) Agostini, F.; Min, S. K.; Abedi, A.; Gross, E. K. U. Quantum-classical non-adiabatic dynamics: Coupled- vs. independent-trajectory methods. *J. Chem. Theory Comput.* **2016**, *12*, 2127–2143.

(61) Curchod, B. F. E.; Agostini, F.; Gross, E. K. U. An Exact Factorization Perspective on Quantum Interferences in Nonadiabatic Dynamics. *J. Chem. Phys.* **2016**, *145*, 034103.

(62) Suzuki, Y.; Watanabe, K. Bohmian mechanics in the exact factorization of electron-nuclear wave functions. *Phys. Rev. A* **2016**, *94*, 032517.

(63) Izmaylov, A. F.; Franco, I. Entanglement in the Born-Oppenheimer Approximation. *J. Chem. Theory Comput.* **2017**, doi:10.1021/acs.jctc.6b00959.

(64) Meek, G. A.; Levine, B. G. Wave function continuity and the diagonal Born-Oppenheimer correction at conical intersections. *J. Chem. Phys.* **2016**, *144*, 184109.

(65) Hahn, S.; Stock, G. Quantum-mechanical modeling of the femtosecond isomerization in rhodopsin. *J. Phys. Chem. B* **2000**, *104*, 1146–1149.

(66) Hahn, S.; Stock, G. Femtosecond secondary emission arising from the nonadiabatic photoisomerization in rhodopsin. *Chem. Phys.* **2000**, *259*, 297–312.

(67) Meek, G. A.; Levine, B. G. The best of both Reps—Diabatized Gaussians on adiabatic surfaces. *J. Chem. Phys.* **2016**, *145*, 184103.

(68) Coker, D.; Xiao, L. Methods for molecular dynamics with nonadiabatic transitions. *J. Chem. Phys.* **1995**, *102*, 496.

(69) Bittner, E. R.; Rossky, P. J. Quantum decoherence in mixed quantum-classical systems: Nonadiabatic processes. *J. Chem. Phys.* **1995**, *103*, 8130–8143.

(70) Prezhdo, O. V.; Rossky, P. J. Mean-field molecular dynamics with surface hopping. *J. Chem. Phys.* **1997**, *107*, 825–834.

(71) Tully, J. C. Mixed quantum classical dynamics. *Faraday Discuss.* **1998**, *110*, 407.

(72) Kapral, R.; Ciccotti, G. Mixed quantum-classical dynamics. *J. Chem. Phys.* **1999**, *110*, 8919–8929.

(73) Martens, C. C. Surface hopping by consensus. *J. Phys. Chem. Lett.* **2016**, *7*, 2610–2615.

(74) Feit, M. D.; Fleck, J. A.; Steiger, A. Solution of the Schrödinger equation by a spectral method. *J. Comp. Phys.* **1982**, *47*, 412 – 433.